Thermodynamic Considerations of Direct Oxygen Removal from Titanium by Utilizing the Deoxidation Capability of Rare Earth Metals

TORU H. OKABE, CHENYI ZHENG, and YU-KI TANINOUCHI

Oxygen removal from metallic Ti is extremely difficult and, currently, there is no commercial process for effectively deoxidizing Ti or its alloys. The oxygen concentration in Ti scraps is normally higher than that in virgin metals such as in Ti sponges produced by the Kroll process. When scraps are remelted with virgin metals for producing primary ingots of Ti or its alloys, the amount of scrap that can be used is limited owing to the accumulation of oxygen impurities. Future demands of an increase in Ti production and of mitigating environmental impacts require that the amount of scrap recycled as a feed material of Ti ingots should also increase. Therefore, it is important to develop methods for removing oxygen directly from Ti scraps. In this study, we evaluated the deoxidation limit for β-Ti using Y or light rare earth metals (La, Ce, Pr, or Nd) as a deoxidant. Thermodynamic considerations suggest that extra-low-oxygen Ti, with an oxygen concentration of 100 mass ppm or less can be obtained using a molten salt equilibrating with rare earth metals. The results presented herein also indicate that methods based on molten salt electrolysis for producing rare earth metals can be utilized for effectively and directly deoxidizing Ti scraps.

https://doi.org/10.1007/s11663-018-1172-4

I. INTRODUCTION

METALLIC Ti has a strong binding affinity with oxygen.[1] Furthermore, as shown in Figure 1, oxygen is highly soluble in metallic Ti.[2,3] At 1300 K (1027 °C), the solubility limit of oxygen in β-Ti is approximately 1 mass pct and in α-Ti, the solubility of oxygen is as high as 14 mass pct. Due to these inherent properties, it is well known that deoxidation of metallic Ti is extremely difficult.

Oxygen dissolved in metallic Ti cannot be removed by employing vacuum melting processes such as electron beam melting and vacuum arc melting. The oxygen content in Ti usually increases during melting, casting, and machining processes. As shown in Figure 2,[4] the oxygen content in typical Ti scrap is usually higher than in virgin metals (300 to 2000 mass ppm) for producing ingots, such as the Ti sponge produced by the Kroll process. Ti scraps often contain oxygen concentrations ranging between 2000 and 4000 mass ppm (0.2 to 0.4 mass pct). Considering the high production cost of metallic Ti, it is desirable to remelt scraps with virgin metals to produce primary ingots of Ti or its alloys. However, the usage of scrap as a raw material increases the oxygen level of the resultant Ti ingots. Commercial processes that can effectively and directly deoxidize Ti have not yet been established. Therefore, scraps with relatively high oxygen contents cannot be reused as raw material for the production of Ti ingots.

The demand for Ti and its alloys has been increasing in various fields and particularly in the aerospace industry. Thus, the recycling of Ti scraps as a raw material for primary ingots has become more important, and the development of effective deoxidation processes for Ti scraps is essential to meet the future demand. Significant attention has been focused on developing methods for the direct removal of oxygen from Ti, and many techniques have been proposed and examined.[4–41] For example, there are many reports on the deoxidation of solid Ti using Ca as a deoxidant.[7–15,20,24–27,29,33–35,37] Oxygen removal during melting process using Ca,[31,32] Al,[28] and H_2[30,36] as deoxidants was also studied. More recently, deoxidation with Mg under a H_2 atmosphere was reported and gained a significant amount of attention in the field.[38,40,41]

TORU H. OKABE is with the Institute of Industrial Science, The University of Tokyo, 4-6-1 Komaba, Meguro-ku, Tokyo 153-8505, Japan. Contact e-mail: okabe@iis.u-tokyo.ac.jp CHENYI ZHENG is with the Institute of Industrial Science, The University of Tokyo and also with the Department of Materials Engineering, Graduate School of Engineering, The University of Tokyo, 7-3-1 Hongo, Bunkyo-ku, Tokyo 113-8656, Japan. YU-KI TANINOUCHI is with the Institute of Industrial Science, The University of Tokyo

Manuscript submitted April 12, 2017.
Article published online February 12, 2018.

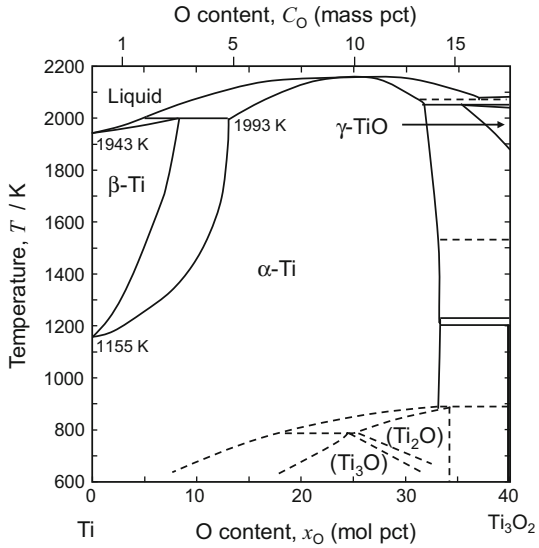

Fig. 1—Binary phase diagram of the Ti-O system adapted from Refs. [2,3].

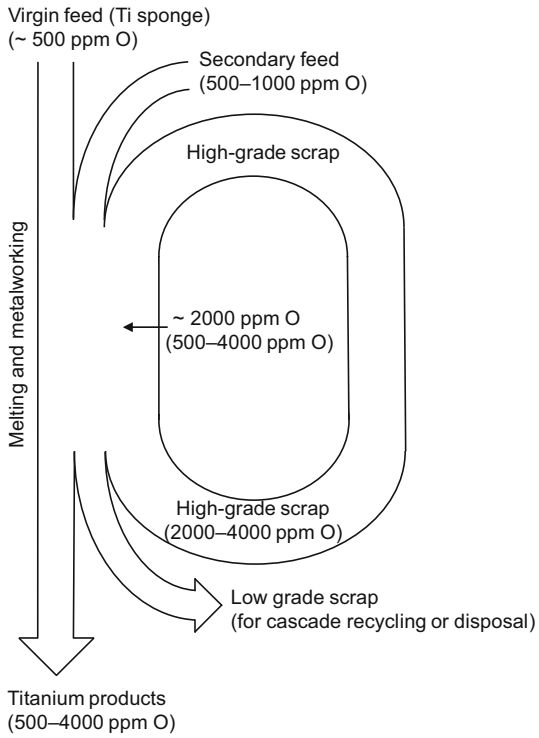

Fig. 2—Material flow of Ti and its alloys with respect to the oxygen concentration. This figure is reprinted with permission from Ref. [4].

Figure 3 illustrates the principles of representative deoxidation methods that can remove oxygen directly from solid Ti.[6] Based on the reactions shown in Figure 3, the oxygen concentration in Ti can be reduced to 500 mass ppm or less in principle. However, the deoxidation techniques involving these reactions have drawbacks limiting their practical application. For example, solid-state electrotransport (Figure 3(a)) has

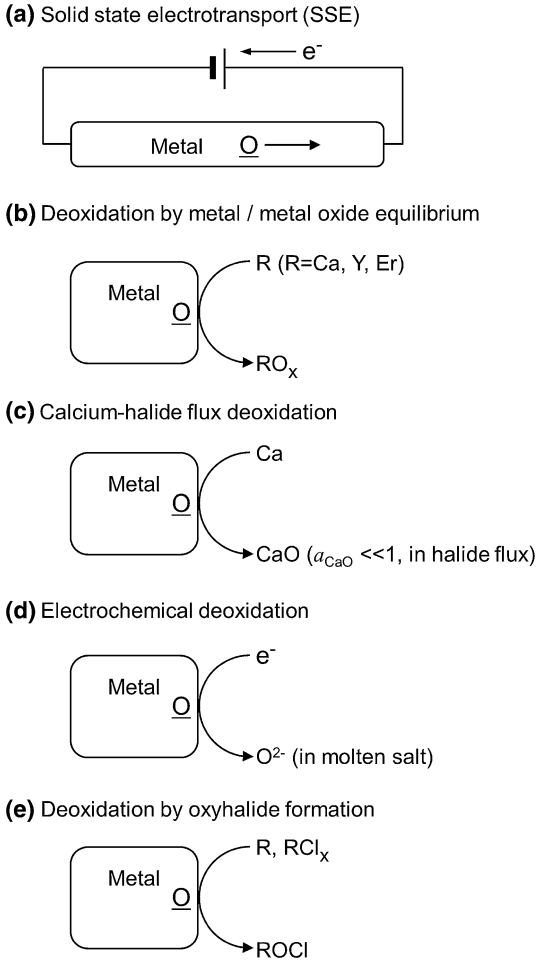

Fig. 3—Principles of representative solid-state purification methods that are capable of reducing the oxygen content in solid Ti to 500 ppm or less. Oxygen removal on the basis of (*a*) solid-state electrotransport technique, (*b*) metal/metal oxide equilibrium, (*c*) calcium-halide flux deoxidation technique, (*d*) electrochemical deoxidation technique, and (*e*) oxyhalide formation. This figure is reprinted with permission from Ref. [6].

considerable limitations in terms of the initial impurity level and sample geometry, and is only applicable to the production of small high-purity specimens. As for deoxidation based on metal/metal oxide equilibria (Figure 3(b)), the number of potential deoxidants is limited. Furthermore, this technique is not suitable for removing large amounts of oxygen. In the past, the RMI Titanium Company (USA) developed an industrial deoxidation process known as the DOSS process that is based on deoxidation using a Ca/CaO equilibrium.[15] However, to the best of our knowledge, the DOSS and similar processes are not currently used on an industrial scale. In calcium-halide flux deoxidation (Figure 3(c)), the oxygen level of Ti can be reduced to approximately 50 mass ppm because the activity of the deoxidation reaction product (CaO) decreases as a result of dissolution into the molten salt flux.[10,12,13,29] However, the ultimate deoxidation limit depends on the amount of deoxidation products generated during processing and on the amounts of oxygen impurities present in the used flux. Therefore, the removal of a large amount of oxygen

is difficult using this process. When the electrochemical deoxidation method (Figure 3(d)) is used, the accumulation of oxygen impurities in the reaction system can be prevented because the O^{2-} generated from the Ti scarp can be removed via conversion to CO_x gas at the carbon anode.[5,16] However, the drawbacks of high electricity consumption and long processing times are often encountered when employing this method. It is also noteworthy that new Ti reduction processes, such as the FFC[42] and OS[43] processes, have been developed based on electrolysis in the $CaCl_2$ molten salt.

Rare earth metals exhibit extremely strong binding affinities to oxygen and are strong deoxidants. For example, under the Y/Y_2O_3 equilibrium at approximately 1200 K (927 °C), Ti with 100 mass ppm of oxygen impurities can be obtained.[6,21] Furthermore, the possibility of deoxidation by equilibrating in the presence of rare earth metals (M), their chlorides (MCl_3), and their oxychlorides (MOCl) has been previously investigated.[20] For example, the chemical potential of oxygen (oxygen partial pressure, p_{O_2}) under the $Nd/NdOCl/NdCl_3$ equilibrium, was reported to be as low as 10^{-51} atm at 1100 K (827 °C). This low p_{O_2} atmosphere would be ideal for deoxidizing Ti.

The above-mentioned studies suggest that rare earth metals can be used as effective deoxidants for Ti. However, only recently industrial production processes for rare earth metals have been developed, precluding the practical utilization of rare earth metals for deoxidizing Ti in the past.

During the last 30 years, the demand for rare earth alloy magnets has been steadily increasing.[44] As a result, the production of rare earth metals and their alloys has been increasing to meet the demand. In particular, the production of Y and light rare earth metals such as La, Ce, Pr, and Nd has increased significantly. Currently, Y and light rare earth metals have the potential to be used as deoxidants in industrial Ti deoxidation processes. The demand for rare earth metals such as Y is relatively low compared to Nd, and continued improvements in their production processes may result in excess supply in the future. It also should be noted that when rare earth metals are used for deoxidizing scraps, the reaction products, such as rare earth metal oxides and oxychlorides, can be reused as raw materials for the production of rare earth metals.

In most cases, rare earth metals and their alloys are produced by molten salt electrolysis.[44,45] Figure 4 shows an image and schematic of a typical industrial electrolysis cell for producing rare earth metals. Table I lists the typical conditions used in industrial electrolysis.[44,46–48] In current industrial processes, rare earth oxides are often added to molten fluoride (in a MF_3–LiF-based bath) as a feed material and are reduced electrochemically. Rare earth metals can also be obtained by molten chloride electrolysis. In the past, mischmetal, which is a mixture of rare earth metals, was commercially produced by molten chloride electrolysis. However, owing to technical issues such as low energy efficiency, chloride electrolysis is rarely used nowadays for producing rare earth metals.

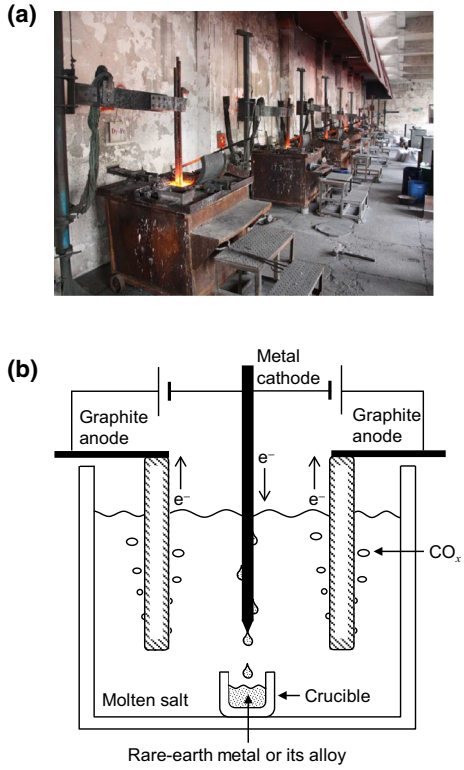

Fig. 4—(*a*) Photograph and (*b*) schematic illustration of a typical electrolysis cell used for producing rare earth metals.

The production capacity of rare earth metals using molten salt electrolysis has been steadily increasing, and overproduction of Y and other light rare earth metals may occur in the future. In light of this prospect, in this study, the deoxidation limit for β-Ti was analyzed when using Y or light rare earth metals (La, Ce, Pr, or Nd) as deoxidants. Furthermore, the feasibility of Ti scrap deoxidation using industrial electrolysis techniques is discussed.

II. PHASE DIAGRAMS AS A FUNCTION OF CHEMICAL POTENTIAL OF OXYGEN AND CHLORINE

Table II lists the standard Gibbs energies of formation ($\Delta G^\circ_{f,i}$) for the rare earth oxides, chlorides, and oxychlorides used in this study. The reliability of the reported thermodynamic data for rare earth compounds is often low. In particular, the data for MOCl have significant uncertainty because the research on MOCl has been quite limited. The thermodynamic data for YOCl used in this study were reported by Patrikeev et al. in 1973.[49] The data for LaOCl and NdOCl were extracted from the database.[1] The thermodynamic data for CeOCl and PrOCl are quite limited. In this study, the $\Delta G^\circ_{f,i}$ for CeOCl and PrOCl have been assessed based on the standard enthalpy of formation at 298 K (25 °C) of the corresponding compounds ($\Delta H^\circ_{f,i,298K}$)[50] and the Gibbs energy function of the formation of LaOCl

Table I. Typical Conditions Used in the Industrial Electrolysis For Producing Rare Earth Metals and Their Alloys

	Y	La	Ce	Pr	Nd	Nd-Fe Alloy
Electrolyte composition	YF_3-LiF	LaF_3-LiF*	CeF_3-LiF-BaF_2	PrF_3-LiF**	NdF_3-LiF†	NdF_3-LiF
Feed	Y_2O_3	La_2O_3	CeO_2	Pr_2O_3	Nd_2O_3	Nd_2O_3
Cathode	W	W	Mo	W	W	Fe
Anode	graphite	graphite	graphite	graphite	graphite	graphite
Electrode distance, d/cm	NA	10 to 15	NA	10 to 15	10 to 15	NA
Electrolysis temp, T/K (°C)	1123 to 1273 (850 to 1000)	1223 to 1273 (950 to 1000)	NA	1273 to 1323 (1000 to 1050)	1323 to 1353 (1050 to 1080)	NA
Electrolysis voltage, E/V	NA	8 to 10	NA	8 to 10	8 to 10	NA
Electrolysis current, I/A	600	4000 to 6000, 10000, 25000	1300	4000 to 6000, 10000, 25000	4000 to 6000, 10000, 25000	> 10000
Cathode current density, i_c/A cm^{-2}	NA	~ 1	NA	~ 1	~ 1	NA
Anode current density, i_a/A cm^{-2}	NA	~ 6.5	NA	~ 6.5	~ 6.5	> 1.0
Current efficiency, χ/pct‡	40 to 51	75 to 80	~ 74	75 to 80	75 to 80	> 85
Specific energy consumption, P/kW h kg^{-1}	NA	9.5 to 11	11.2	9.5 to 11	9.5 to 11	NA
Refs.	[47]	[48]	[46]	[48]	[48]	[44]

NA: Data is not available.
*LaF_3:LiF = 85:15 in mass ratio.
**PrF_3:LiF = 90:10 in mass ratio.
†NdF_3:LiF = 90:10 in mass ratio.
‡Cathode reaction.

Table II. Standard Gibbs Energy of Formation of Compounds in the M-O-Cl System

Compound, i	Standard Gibbs Energy of Formation, $\Delta G^\circ_{f,i}$ (J·mol^{-1})		Refs.
$Y_2O_3(s)$	$\Delta G^\circ_{f,i} = -1{,}892{,}000 + T \times 278.1$	1100 to 1500 K (827 to 1227 °C)	[1]
$YCl_3(l)$	$\Delta G^\circ_{f,i} = -941{,}500 + T \times 175.6$	1100 to 1500 K (827 to 1227 °C)	[1]
YOCl(s)	$\Delta G^\circ_{f,i} = -1{,}075{,}000 + T \times 219.5$	1248 to 1375 K (975 to 1102 °C)	[49]
$La_2O_3(s)$	$\Delta G^\circ_{f,i} = -1{,}794{,}000 + T \times 284.8$	1100 to 1500 K (827 to 1227 °C)	[1]
$LaCl_3(s)$	$\Delta G^\circ_{f,i} = -1{,}049{,}000 + T \times 219.7$	1000 to 1131 K (727 to 858 °C)	[1]
$LaCl_3(l)$	$\Delta G^\circ_{f,i} = -989{,}400 + T \times 167.0$	1131 to 1500 K (858 to 1227 °C)	[1]
LaOCl(s)	$\Delta G^\circ_{f,i} = -1{,}002{,}000 + T \times 172.8$	1000 to 1200 K (727 to 973 °C)	[1]
$CeO_2(s)$	$\Delta G^\circ_{f,i} = -1{,}089{,}000 + T \times 208.4$	1100 to 1500 K (827 to 1227 °C)	[1]
$Ce_2O_3(s)$	$\Delta G^\circ_{f,i} = -1{,}789{,}000 + T \times 275.7$	1000 to 1200 K (727 to 927 °C)	[1]
$CeCl_3(l)$	$\Delta G^\circ_{f,i} = -980{,}100 + T \times 172.6$	1100 to 1300 K (827 to 1027 °C)	[1]
CeOCl(s)	$\Delta G^\circ_{f,i} = -990{,}900 + T \times 172.9$	1100 to 1500 K (827 to 1227 °C)	Estimated*
$Pr_2O_3(s)$	$\Delta G^\circ_{f,i} = -1{,}807{,}000 + T \times 284.8$	1100 to 1500 K (827 to 1227 °C)	[1]
$PrCl_3(l)$	$\Delta G^\circ_{f,i} = -983{,}400 + T \times 171.5$	1100 to 1500 K (827 to 1227 °C)	[1]
PrOCl(s)	$\Delta G^\circ_{f,i} = -1{,}004{,}000 + T \times 172.9$	1100 to 1500 K (827 to 1227 °C)	Estimated**
$Nd_2O_3(s)$	$\Delta G^\circ_{f,i} = -1{,}808{,}000 + T \times 281.3$	1100 to 1500 K (827 to 1227 °C)	[1]
$NdCl_3(l)$	$\Delta G^\circ_{f,i} = -967{,}300 + T \times 167.7$	1100 to 1300 K (827 to 1027 °C)	[1]
NdOCl(s)	$\Delta G^\circ_{f,i} = -991{,}800 + T \times 176.4$	900 to 1100 K (627 to 827 °C)	[1]

*Estimated based on Eq. [2].
**Estimated based on Eq. [3].

(Δgef_{LaOCl}). Δgef_{LaOCl} at the absolute temperature T can be calculated using the $\Delta G^\circ_{f,LaOCl}$ at T and $\Delta H^\circ_{f,LaOCl,298K}$ derived from the database[1] as follows:

$$\Delta gef_{LaOCl} = (\Delta G^\circ_{f,LaOCl} - \Delta H^\circ_{f,LaOCl,298K})/T. \quad [1]$$

The $\Delta G^\circ_{f,i}$ values for CeOCl and PrOCl shown in Table II were calculated as follows:

$$\Delta G^\circ_{f,CeOCl} = \Delta H^\circ_{f,CeOCl,298K} + T \cdot \Delta gef_{LaOCl} \quad [2]$$

$$\Delta G^\circ_{f,PrOCl} = \Delta H^\circ_{f,PrOCl,298K} + T \cdot \Delta gef_{LaOCl}. \quad [3]$$

Figures 5 through 9 show the chemical potential diagrams of the M-O-Cl systems at 1300 K (1027 °C),

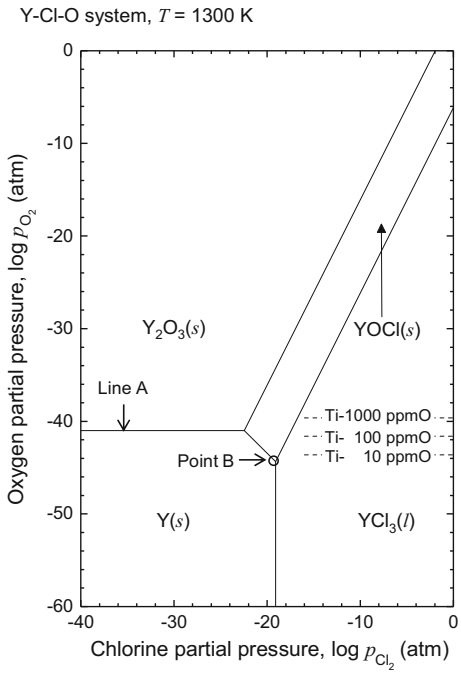

Fig. 5—Potential diagram of the Y-Cl-O system at 1300 K (1027 °C) calculated using the thermodynamic data shown in Table II.

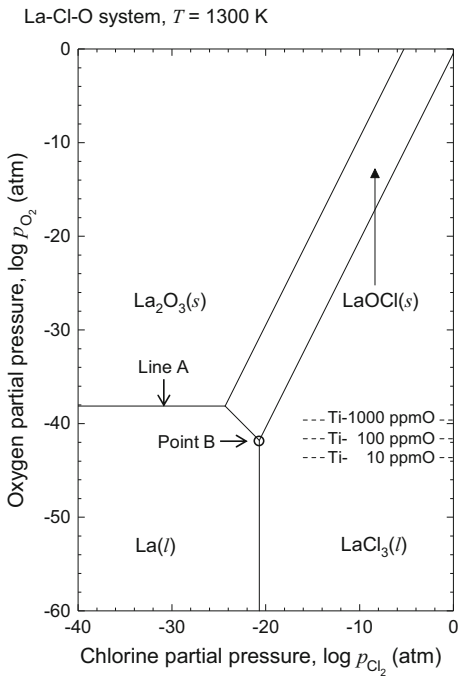

Fig. 6—Potential diagram of the La-Cl-O system at 1300 K (1027 °C) calculated using the thermodynamic data shown in Table II. Temperature dependences of $\Delta G^{\circ}_{f,LaCl_3}$ and $\Delta G^{\circ}_{f,LaOCl}$ shown in Table II were assumed to be established at 1300 K (1027 °C).

calculated using the data listed in Table II. In these diagrams, the vertical axis is the logarithm of p_{O_2} (atm), and the horizontal axis is the logarithm of the chlorine partial pressure (p_{Cl_2} (atm)). In each diagram, a stable region of MOCl is observed. The p_{O_2} determined

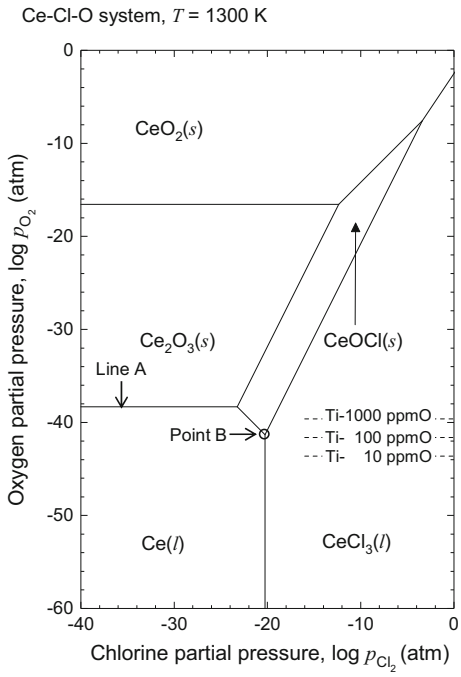

Fig. 7—Potential diagram of the Ce-Cl-O system at 1300 K (1027 °C) calculated using the thermodynamic data shown in Table II. Temperature dependence of $\Delta G^{\circ}_{f,Ce_2O_3}$ shown in Table II was assumed to be established at 1300 K (1027 °C).

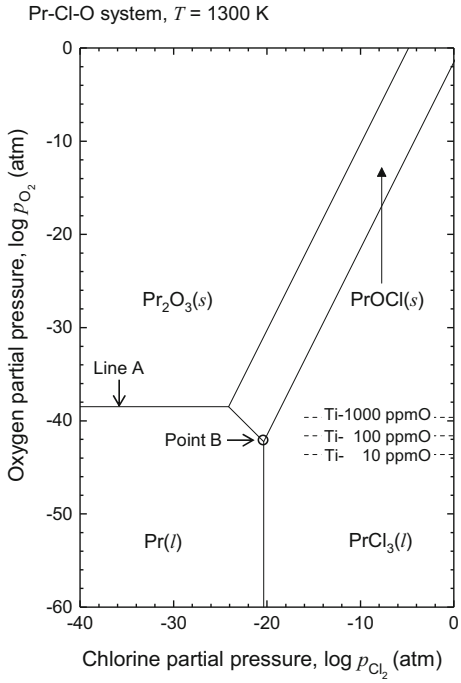

Fig. 8—Potential diagram of the Pr-Cl-O system at 1300 K (1073 °C) calculated using the thermodynamic data shown in Table II.

by the M/M_2O_3 equilibrium (line A in Figures 5 to 9) is extremely low, smaller than 10^{-38} atm. Furthermore, in any system, the p_{O_2} determined by the M/MOCl/MCl_3 equilibrium (point B in Figures 5 to 9) is lower than that

determined by the M/M_2O_3 equilibrium (line A in Figures 5 to 9). For example, the p_{O_2} determined by the Y/Y_2O_3 equilibrium is 10^{-41} atm at 1300 K (1027 °C), meanwhile, the p_{O_2} determined by the $Y/YOCl/YCl_3$ equilibrium is 10^{-44} atm.

Under such an extremely low p_{O_2} achieved by the M/M_2O_3 or $M/MOCl/MCl_3$ equilibria, it should be possible to reduce the oxygen level in metallic Ti. However, as shown in Table III, rare earth metals dissolve in Ti up to a limit of several mass pct at approximately 1300 K (1027 °C).[3] Therefore, when these rare earth metals with high solubility in Ti are used as deoxidants, they might contaminate the final Ti product. After the deoxidation treatment, the Ti scrap is expected to be remelted under vacuum by electron beam melting or another melting method to produce the Ti ingots. During this remelting process, rare earth metals contaminating the Ti scrap might be evaporated and removed.

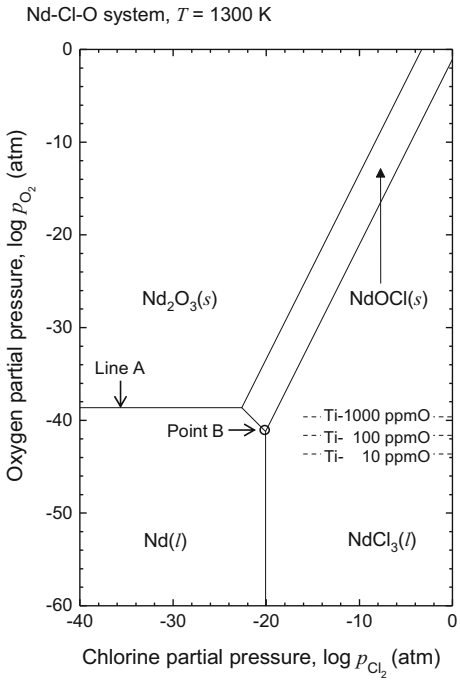

Fig. 9—Potential diagram of the Nd-Cl-O system at 1300 K (1073 °C) calculated using the thermodynamic data shown in Table II. Temperature dependence of $\Delta G^\circ_{f,NdOCl}$ shown in Table II was assumed to be established at 1300 K (1027 °C).

III. THE DEOXIDATION LIMIT OF *B*-TI UNDER THE EQUILIBRIUM OF RARE EARTH METALS AND THEIR OXIDES

In this section, the deoxidation limits for reactions yielding rare earth oxides (M_2O_3) are discussed (see Figure 3(b)). The deoxidation reaction of Ti by rare earth metals can be expressed by the following reaction:

$$\begin{array}{l} \text{O (in Ti)} + 2/3\ \text{M (in flux)} \rightarrow 1/3\ M_2O_3\text{(in flux)} \\ \text{M: Deoxidant (Y, La, Ce, Pr or Nd)} \end{array} \quad [4]$$

The relationship between the concentration of oxygen in β-Ti ($[O]_{Ti}$ (mass pct)) and p_{O_2} can be expressed as follows:

$$1/2\ O_2(g) = O\ (1\ \text{mass pct, in Ti}) \quad [5]$$

$$\Delta G^\circ_{1,Ti} = -2.303 \cdot RT \log \frac{f_O \cdot [O]_{Ti}}{P^{1/2}_{O_2}} \quad [6]$$

$$\begin{array}{r} \Delta G^\circ_{1,Ti} = -583000 + 88.5T(\text{J}) \\ [1173 - 1373\,\text{K}(900 - 1100\,^\circ\text{C})], \end{array} \quad [7]$$

where oxygen dissolved in Ti is expressed relative to the 1 mass pct standard state, $\Delta G^\circ_{1,Ti}$ is the standard Gibbs energy of oxygen dissolution in β-Ti, R is the gas constant, T is the absolute temperature, and f_O is the Henrian activity coefficient for oxygen dissolved in β-Ti. Given that the oxygen dissolved in Ti obeys Henry's law, the value of f_O is considered to be unity.

Meanwhile, the p_{O_2} determined by the M/M_2O_3 equilibrium is related to the standard Gibbs energy of M_2O_3 formation ($\Delta G^\circ_{f,M_2O_3}$, listed in Table II) and calculated as follows:

$$2M(s \text{ or } l) + 3/2\ O_2(g) = M_2O_3(s) \quad [8]$$

Table III. Solubility of Oxygen and Rare Earth Metals in *β*-Ti[2,3]

Temperature, T/K (°C)	Solubility of Element i in β-Ti, $C_{i,\text{in Ti}}$ (Mass Pct)					
	O	Y	La	Ce	Pr	Nd
1200 (927)	0.3	0.4	1.3	1.4	(2)	1.3
1300 (1027)	0.9	0.7	2.0	2.0	(2)	2.0
1400 (1127)	1.3	1.0	2.7	2.6	(2)	2.6
1500 (1227)	1.7	1.5	3.6	3.3	(2)	3.2

Values in parentheses include large uncertainties.

Table IV. Summary of Standard Gibbs Energy of the Deoxidation Reaction Yielding M_2O_3

Deoxidation Reaction*	Standard Gibbs Energy Change of the Deoxidation Reaction from 1173 to 1373 K (900 to 1100 °C), $\Delta G^\circ_{deox,M_2O_3}$/J**
O(1 mass pct, in Ti) + 2/3 Y(s) = 1/3 Y_2O_3(s)	$\Delta G^\circ_{deox,Y_2O_3} = -48{,}000 + T \times 4.2$
O(1 mass pct, in Ti) + 2/3 La(s or l) = 1/3 La_2O_3(s)	$\Delta G^\circ_{deox,La_2O_3} = -15{,}000 + T \times 6.4$
O(1 mass pct, in Ti) + 2/3 Ce(l) = 1/3 Ce_2O_3(s)	$\Delta G^\circ_{deox,Ce_2O_3} = -13{,}000 + T \times 3.4$
O(1 mass pct, in Ti) + 2/3 Pr(s or l) = 1/3 Pr_2O_3(s)	$\Delta G^\circ_{deox,Pr_2O_3} = -19{,}000 + T \times 6.4$
O(1 mass pct, in Ti) + 2/3 Nd(s or l) = 1/3 Nd_2O_3(s)	$\Delta G^\circ_{deox,Nd_2O_3} = -20{,}000 + T \times 5.3$

*Melting points of La, Pr, and Nd are 1193, 1204, and 1289 K (920, 931, and 1016 °C), respectively.
**$\Delta G^\circ_{deox,M_2O_3} = 1/3\Delta G^\circ_{f,M_2O_3} - \Delta G^\circ_{1,Ti}$.
Data of $\Delta G^\circ_{f,M_2O_3}$ are shown in Table II. Temperature dependence of $\Delta G^\circ_{f,Ce_2O_3}$ was assumed to be established above 1200 K (927 °C).

Table V. Oxygen Concentration in β-Ti Under M/M_2O_3 Equilibrium

Temperature, T/K (°C)	Theoretical Oxygen Concentration in β-Ti Under M/M_2O_3 Equilibrium at T, C_O (mass ppm)				
	Y	La	Ce	Pr	Nd
1200 (927)	130	4800	4100	3200	2500
1300 (1027)	200	5400	4500	3700	3000
1400 (1127)	270*	6000*	4900*	4200*	3500*
1500 (1227)	350*	6500*	5300*	4700*	3900*

The oxygen concentration was calculated using the $\Delta G^\circ_{deox,M_2O_3}$ values shown in Table IV.
*Calculated under the assumption that temperature dependence of $\Delta G^\circ_{deox,M_2O_3}$ holds above 1373 K (1100 °C).

$$\Delta G^\circ_{f,M_2O_3} = -2.303 \cdot RT \log \frac{a_{M_2O_3}}{a_M^2 \cdot P_{O_2}^{3/2}}, \quad [9]$$

where a_i is the activity of substance i. Lines A in Figures 5 through 9 correspond to the p_{O_2} when the temperature is 1300 K (1027 °C) and both a_M and $a_{M_2O_3}$ are unity.

Based on Eqs. [5] and [8], the deoxidation of β-Ti under the M/M_2O_3 equilibrium can be expressed as follows:

$$O\ (1\ \text{mass pct, in Ti}) + 2/3\ M\ (s \text{ or } l) = 1/3\ M_2O_3(s) \quad [10]$$

$$\Delta G^\circ_{deox,M_2O_3} = 1/3\Delta G^\circ_{f,M_2O_3} - \Delta G^\circ_{1,Ti} \quad [11]$$

$$\Delta G^\circ_{deox,M_2O_3} = -2.303 \cdot RT \log \frac{a_{M_2O_3}^{1/3}}{f_O \cdot [O]_{Ti} \cdot a_M^{2/3}}. \quad [12]$$

Table IV summarizes the $\Delta G^\circ_{deox,M_2O_3}$ values calculated from Eq. [11].

When the oxygen dissolved in β-Ti is assumed to obey Henry's law ($f_O = 1$), and when the a_M and $a_{M_2O_3}$ are given, the oxygen concentration in β-Ti under the M/M_2O_3 equilibrium can be calculated from Eq. [12]. Table V shows the calculated concentrations of oxygen in β-Ti under the M/M_2O_3 equilibrium, when both a_M and $a_{M_2O_3}$ are unity. From this data, it is clear that Y is the strongest deoxidant among Y, La, Ce, Pr, and Nd. By using Y as the deoxidant, the concentration of oxygen in β-Ti can be reduced to approximately 200 mass ppm at 1300 K (1027 °C). When the $a_{M_2O_3}$can be maintained at low values ($a_{M_2O_3} \ll 1$) by using a flux (or molten salt), the theoretical deoxidation limit of Ti became lower than that listed in Table V.

IV. THE DEOXIDATION LIMIT OF *B*-TI USING THE REACTION FOR PRODUCING RARE EARTH OXYCHLORIDES

In this section, the deoxidation limit of β-Ti using the oxygen removal reaction where the oxygen is eliminated as a rare earth oxychloride (see Figure 3(e)) is evaluated. As shown in Figures 5 through 9, the value of p_{O_2}determined by the $M/MOCl/MCl_3$ equilibrium (point B) is lower than that determined by the M/M_2O_3 equilibrium (line A). Hence, deoxidation in molten MCl_3 using M as the deoxidant is likely to more efficiently reduce the oxygen levels in Ti.

The deoxidation reaction during which the oxygen in Ti is converted into MOCl can be expressed as follows:

$$O\ (\text{in Ti}) + 2/3\ M\ (\text{in flux}) + 1/3\ MCl_3(\text{in flux}) \rightarrow MOCl\ (\text{in flux})$$

M: Deoxidant (Y, La, Ce, Pr, or Nd). [13]

Table VI. Summary of Standard Gibbs Energy of the Deoxidation Reaction Yielding MOCl

Deoxidation Reaction*	Standard Gibbs Energy Change of the Deoxidation Reaction from 1173 to 1373 K (900 to 1100 °C), $\Delta G^\circ_{\text{deox,MOCl}}$/J**
O(1 mass pct, in Ti) + 2/3 Y(s) + 1/3 YCl_3(l) = YOCl(s)	$\Delta G^\circ_{\text{deox,YOCl}} = -180{,}000 + T \times 72$
O(1 mass pct, in Ti) + 2/3 La(s or l) + 1/3 $LaCl_3$(l) = LaOCl(s)	$\Delta G^\circ_{\text{deox,LaOCl}} = -89{,}000 + T \times 29$
O(1 mass pct, in Ti) + 2/3 Ce(l) + 1/3 $CeCl_3$(l) = CeOCl(s)	$\Delta G^\circ_{\text{deox,CeOCl}} = -81{,}000 + T \times 27$
O(1 mass pct, in Ti) + 2/3 Pr(s or l) + 1/3 $PrCl_3$(l) = PrOCl(s)	$\Delta G^\circ_{\text{deox,PrOCl}} = -93{,}000 + T \times 27$
O(1 mass pct, in Ti) + 2/3 Nd(s or l) + 1/3 $NdCl_3$(l) = NdOCl(s)	$\Delta G^\circ_{\text{deox,NdOCl}} = -86{,}000 + T \times 32$

*Melting points of La, Pr, and Nd are 1193, 1204, and 1289 K (920, 931, and 1016 °C), respectively.
**$\Delta G^\circ_{\text{deox,MOCl}} = \Delta G^\circ_{\text{deox,MOCl}} - 1/3\Delta G^\circ_{\text{f,MCl}_3} - \Delta G^\circ_{\text{1,Ti}}$.
Data of $\Delta G^\circ_{\text{f,MCl}_3}$ and $\Delta G^\circ_{\text{f,MOCl}}$ are shown in Table II. Temperature dependence of $\Delta G^\circ_{\text{f,LaOCl}}$, $\Delta G^\circ_{\text{f,CeCl}_3}$, $\Delta G^\circ_{\text{f,NdCl}_3}$, $\Delta G^\circ_{\text{f,NdOCl}}$ shown in Table II was assumed to be established up to 1373 K (1100 °C).

Table VII. Oxygen Concentration in β-Ti Under M/MOCl/MCl_3 Equilibrium

Temperature, T/K (°C)	Theoretical Oxygen Concentration in β-Ti Under M/MOCl/MCl_3 Equilibrium at T, C_O (Mass ppm)				
	Y	La	Ce	Pr	Nd
1200 (927)	0.84	44	77	23	85
1300 (1027)	3.4	87	140	47	160
1400 (1127)	11*	160*	240*	87*	290*
1500 (1227)	31*	260*	390*	150*	480*

The oxygen concentrations were calculated using the $\Delta G^\circ_{\text{deox,MOCl}}$ values shown in Table VI.
*Calculated under the assumption that temperature dependence of $\Delta G^\circ_{\text{deox,MOCl}}$ holds above 1373 K (1100 °C).

The p_{O_2} determined by the M/MOCl/MCl_3 equilibrium can be expressed as follows:

$$2/3\ \text{M}(s \text{ or } l) + 1/3\ \text{MCl}_3(s \text{ or } l) + 1/2\ \text{O}_2(g) = \text{MOCl}(s) \quad [14]$$

$$\Delta G^\circ_{\text{r,MOCl}} = -2.303 \cdot RT \log \frac{a_{\text{MOCl}}}{a_{\text{M}}^{2/3} \cdot a_{\text{MCl}_3}^{2/3} \cdot P_{\text{O}_2}^{1/2}} \quad [15]$$

$$\Delta G^\circ_{\text{r,MOCl}} = \Delta G^\circ_{\text{f,MOCl}} - 1/3\Delta G^\circ_{\text{f,MCl}_3}. \quad [16]$$

Points B in Figures 5 through 9 correspond to the p_{O_2} when the temperature is 1300 K (1027 °C) and a_M, a_{MCl_3}, and a_{MOCl} are unity.

According to Eqs. [5] and [14], the thermodynamic parameters for the deoxidation reaction that yields MOCl can be calculated as follows:

$$\text{O (1mass pct, in Ti)} + 2/3\ \text{M}\ (s \text{ or } l) + 1/3\ \text{MCl}_3(s \text{ or } l) = \text{MOCl}\ (s) \quad [17]$$

$$\Delta G^\circ_{\text{deox,MOCl}} = -2.303 \cdot RT \log \frac{a_{\text{MOCl}}}{f_{\text{O}} \cdot [\text{O}]_{\text{Ti}} \cdot a_{\text{M}}^{2/3} \cdot a_{\text{MCl}_3}^{1/3}} \quad [18]$$

$$\Delta G^\circ_{\text{deox,MOCl}} = \Delta G^\circ_{\text{r,MOCl}} - \Delta G^\circ_{\text{1,Ti}} = \Delta G^\circ_{\text{f,MOCl}} - 1/3\Delta G^\circ_{\text{f,MCl}_3} - \Delta G^\circ_{\text{1,Ti}}. \quad [19]$$

Table VI lists the $\Delta G^\circ_{\text{deox,MOCl}}$ values calculated using Eq. [7], as well as $\Delta G^\circ_{\text{f,MCl}_3}$ and $\Delta G^\circ_{\text{f,MOCl}}$ values that are listed in Table II.

It is assumed that an excess amount of M and MCl_3 is present in the reaction system ($a_M = 1$ and $a_{MCl_3} = 1$) and that the oxygen in β-Ti obeys Henry's law ($f_O = 1$). Under these assumption, the oxygen concentration in β-Ti under the M/MOCl/MCl_3 equilibrium can be calculated from Eq. [19] at a given a_{MOCl} and T. Table VII lists the calculated results obtained for $a_{MOCl} = 1$. As shown in Table V, light rare earth metals (La, Ce, Pr, and Nd) are less powerful deoxidants than Y. However, under the M/MOCl/MCl_3 equilibrium, the oxygen concentration in Ti can be reduced to 200 mass ppm or less at 1300 K (1027 °C) when using a light rare earth metal as a deoxidant.

V. VAPOR PRESSURE OF RARE EARTH CHLORIDES

Ti scraps often have a complex surface structure. After Ti scraps are deoxidized using molten chloride and then removed from the molten salt bath, a significant quantity of salt is likely to remain attached to their surfaces. Metal chlorides attached to the scrap surfaces can subsequently be removed by wet processing.

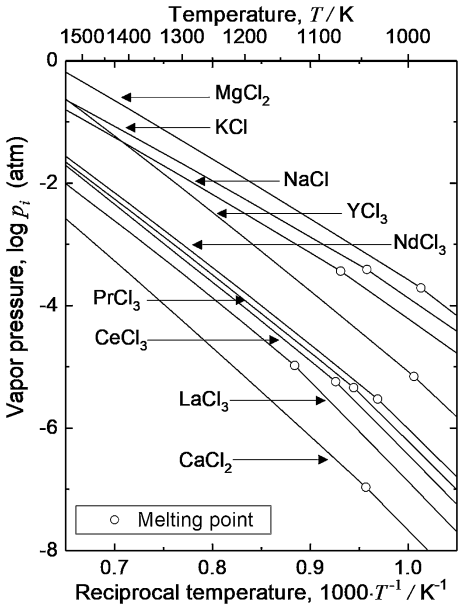

Fig. 10—Temperature dependence of the vapor pressures of selected chlorides.[1,51].

However, this treatment increases the cost associated with processing, because a significant amount of waste solution is generated. Furthermore, the concentration of oxygen in the Ti scraps would likely increase during wet processing. Hence, in the following section, the removal of attached salts using evaporation is discussed.

Figure 10 shows the vapor pressures of some rare earth chlorides as a function of temperature.[1,51] $MgCl_2$ can be easily separated from metallic Ti by evaporation because its volatility is sufficiently high. In fact, during Ti smelting based on the Kroll process, $MgCl_2$ that is generated as a by-product of the Ti reduction step was separated from the Ti sponge by evaporation.[52] Compared with the vapor pressure of $MgCl_2$, that of YCl_3 is nearly one order of magnitude lower. Furthermore, the vapor pressures of $LaCl_3$, $CeCl_3$, $PrCl_3$, and $NdCl_3$ are nearly two orders of magnitude lower than that of $MgCl_2$. Therefore, it is considerably more difficult to remove rare earth chlorides by evaporation. For cleaning the surfaces of scraps after the deoxidation process, rinsing the MOCl and MCl_3 using molten $MgCl_2$, followed by evaporation may be an effective removal method.

VI. DEOXIDATION OF TI USING MOLTEN SALT ELECTROLYSIS OF RARE EARTH METALS

Figure 11 shows the relationship between the oxygen concentration in β-Ti and p_{O_2} between 1200 and 1500 K (927 and 1227 °C). The data at 1400 and 1500 K (1127 and 1227 °C) were calculated by extrapolating the thermodynamic data in Eq. [7].[9] In Figure 11, the theoretical oxygen concentration in β-Ti under the M/M_2O_3 and $M/MOCl/MCl_3$ equilibria (see Tables V and VII) and the Ca/CaO equilibrium[1] are plotted together.

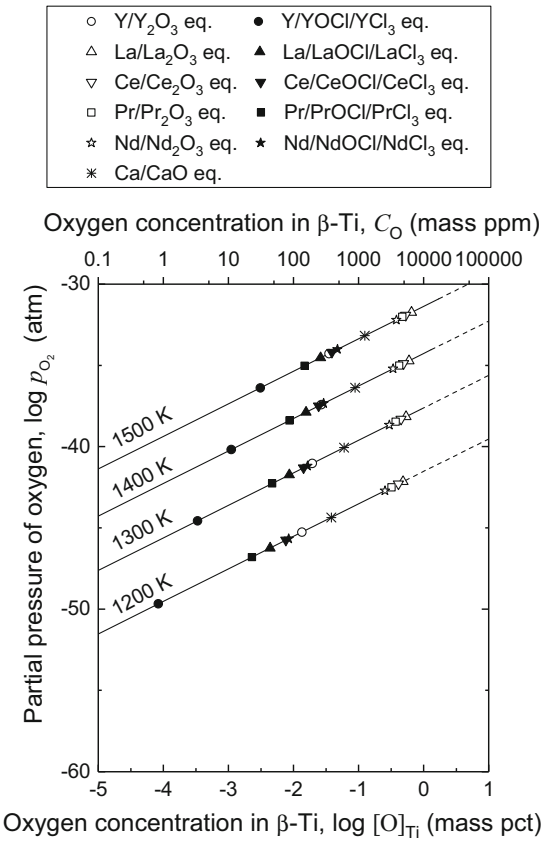

Fig. 11—Relationship between oxygen concentration in β-Ti and the partial pressure of oxygen. Oxygen concentrations determined by the Ca/CaO eq., M/M_2O_3 eq., and $M/MOCl/MCl_3$ eq. (M: Y, La, Ce, Pr, or Nd) are also shown.

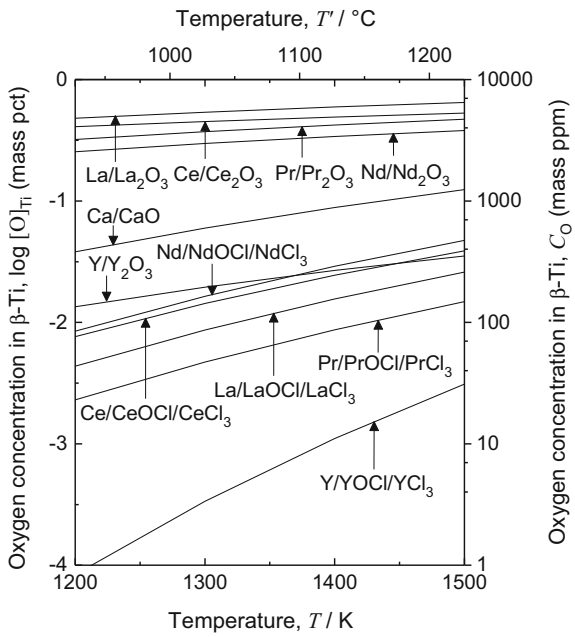

Fig. 12—Temperature dependence of oxygen concentration in β-Ti determined by the M/M_2O_3 and $M/MOCl/MCl_3$ (M: Y, La, Ce, Pr, or Nd) equilibria.

In Figure 12, the oxygen concentration in β-Ti under the M/M_2O_3 and $M/MOCl/MCl_3$ equilibria are plotted as a function of temperature.

As can be seen in Figures 11 and 12, the oxygen levels in Ti can be reduced below 500 mass ppm by using the Y/Y_2O_3 equilibrium. Meanwhile, when the activity of the reaction product M_2O_3 ($a_{M_2O_3}$) is unity, the oxygen concentration in Ti cannot be reduced under 1000 mass ppm by using La, Ce, Pr, or Nd as a deoxidant. Currently, rare earth metals are produced by oxide electrolysis in a molten fluoride bath, as shown in Table I and Figure 4. In this industrial electrolytic cell, the pure metal or alloy of rare earths is deposited on the cathode. Furthermore, the value of $a_{M_2O_3}$ can be maintained at less than 1, because the molten fluoride acts as a flux for M_2O_3. In particular, the value $a_{M_2O_3}$ around the cathode is estimated to be quite low. Therefore, the industrial electrolytic cell is expected to be applicable for the efficient deoxidation of Ti scraps, and low oxygen Ti may be obtained even when light rare earth metals, such as Nd, are used as a deoxidant.

The oxygen level in Ti can be reduced below 500 mass ppm by utilizing the $M/MOCl/MCl_3$ equilibrium. Especially, under the $Y/YOCl/YCl_3$ equilibrium the oxygen level, in principle, can be reduced to 10 mass ppm or less at approximately 1300 K (1027 °C). During the electrolysis of molten chloride to yield rare earth metals, the $M/MOCl/MCl_3$ equilibrium is expected to be established around the cathode. Hence, when Ti scraps can be kept near the cathode, oxygen impurities will be removed efficiently. However, it is essential to monitor for the contamination of the Ti scraps by the rare earth metals used in this process (see Table III).

Figures 11 and 12 also indicate that deoxidization is likely to be more effective at lower temperatures when the same deoxidant is used. However, the diffusion rate of oxygen in Ti is much slower at lower temperatures.[53] Therefore, the optimal process temperature is estimated to be around 1300 K (1027 °C), which corresponds to the operational temperature of electrolysis of rare earth metals. The production volume and global production capacity for rare earth metals by molten salt electrolysis are expected to continually increase as the related technologies are further developed. Therefore, it will be industrially feasible to achieve the deoxidation of Ti scraps utilizing electrolysis techniques for producing rare earth metals.

When Ti scraps are deoxidized by using the molten salt electrolysis used for producing rare earth metals, the oxygen in the scrap is dissolved as O^{2-} in the molten salt and then removed as CO_x gas at the carbon anode. Thus, the accumulation of oxygen in the molten salt can be prevented. The oxygen removal capacity of this electrochemical deoxidation technique is inherently high, and Ti with extremely low oxygen content can be obtained. However, when deoxidation is performed in currently used electrolysis cells, large-scale processing may be technically difficult due to the limitations on the placement of electrodes and their co-localization with Ti scraps. It is also possible to deoxidize Ti scraps using rare earth metals that are separately produced by an electrochemical or other methods. The deoxidation limit when using a rare earth metal is high compared to the electrochemical method because of the accumulation of the deoxidation product. However, this chemical deoxidation technique is advantageous for processing a large amount of scraps and preventing contamination by other impurities.

VII. CONCLUSION

From a thermodynamic viewpoint, the possibility of the direct removal of oxygen from β-Ti using Y and light rare earth metals (La, Ce, Pr, and Nd) as deoxidants was discussed. Under the Y/Y_2O_3 equilibrium at 1300 K (1027 °C), a highly reducing atmosphere with an oxygen partial pressure of 10^{-41} atm can be obtained, facilitating the reduction of oxygen concentration in Ti to 200 mass ppm. Moreover, under the $Y/YOCl/YCl_3$ equilibria at 1300 K (1027 °C), an oxygen partial pressure lower than that of the Y/Y_2O_3 equilibrium can be achieved, and the oxygen level in Ti can be theoretically reduced to 10 mass ppm or less. Light rare earth metals were shown to be weak deoxidants compared with Y. In the case of the M/M_2O_3 equilibrium under 1300 K (1027 °C) and when the activity of the reaction product (M_2O_3) is unity, the oxygen concentration in Ti cannot be reduced under 1000 mass ppm by using La, Ce, Pr, or Nd as a deoxidant. However, under the $M/MOCl/MCl_3$ equilibrium, the oxygen concentration in Ti can be reduced to 200 mass ppm or less using La, Ce, Pr, or Nd as a deoxidant. These results suggest that deoxidation of Ti scraps can be performed using molten salt electrolysis of Y or light rare earth metals in the future.

ACKNOWLEDGMENTS

The authors are grateful to Professors Hongmin Zhu and Osamu Takeda at Tohoku University for their valuable comments and helpful suggestions. This work was financially supported by the Japan Society for the Promotion of Science (JSPS) through a Grant-in-Aid for Scientific Research (S) (KAKENHI Grant No. 26220910).

REFERENCES

1. I. Barin: *Thermochemical Data of Pure Substance*, 3rd ed., Wiley-VCH, Weinheim, Germany, 1995.
2. J.L. Murray and H.A. Wriedt: *J. Phase Equilib.*, 1987, vol. 8, pp. 148–65.
3. T.B. Massalski: *Binary Alloy Phase Diagrams*, 2nd ed., ASM International, Materials Park, OH, 1990.
4. Y. Taninouchi, Y. Hamanaka, and T.H. Okabe: *Metall. Mater. Trans. B*, 2016, vol. 47B, pp. 3394–404.
5. T.H. Okabe, Y. Hamanaka, and Y. Taninouchi: *Faraday Discuss.*, 2016, vol. 190, pp. 109–26.
6. Y. Waseda and M. Isshiki eds.: *Purification Process and Characterization of Ultra High Purity Metals*, 3rd ed., Springer, Berlin, 2001, pp. 3–37.
7. K. Ono and S. Miyazaki: *J. Jpn Inst. Met.*, 1985, vol. 49, pp. 871–75 (in Japanese).

8. R.L. Fisher: US Patent, 4923531A, 1990.
9. T.H. Okabe, R.O. Suzuki, T. Oishi and K. Ono: *Mater. Trans., JIM*, 1991, vol. 32, pp. 485–88.
10. T.H. Okabe, R.O. Suzuki, T. Oishi, and K. Ono: *J. Iron Steel Inst. Jpn.*, 1991, vol. 77, pp. 93–99 (in Japanese).
11. R.L. Fisher: US Patent, 5022935, 1991.
12. T.H. Okabe, T. Oishi, and K. Ono: *J. Alloys Compd.*, 1992, vol. 184, pp. 43–56.
13. T.H. Okabe, T. Oishi, and K. Ono: *Met. Trans. B*, 1992, vol. 23, pp. 583–90.
14. R.L. Fisher and S.R. Seagle: US Patent, No. 5211775 A, 1993.
15. R.L. Fisher and S.R. Seagle: *Proceedings of 7th World Conference on Titanium*, 1993, vol. 3, pp. 2265–72.
16. T.H. Okabe, M. Nakamura, T. Oishi, and K. Ono: *Met. Trans. B*, 1993, vol. 24, pp. 449–55.
17. M. Nakamura, T.H. Okabe, T. Oishi, and K. Ono: *Proceedings of International Symposium on Molten Salt Chemistry and Technology*, 1993, pp. 529–40.
18. T.H. Okabe, T. Deura, T. Oishi, K. Ono, and D.R. Sadoway: *Metall. Mater. Trans. B*, 1996, vol. 27B, pp. 841–47.
19. T.H. Okabe, T. Deura, T. Oishi, K. Ono, and D.R. Sadoway: *J. Alloys Compd.*, 1996, vol. 237, pp. 150–54.
20. T.H. Okabe, K. Hirota, Y. Waseda, and K.T. Jacob: *J. Min. Mater. Process. Inst. Jpn.*, 1998, vol. 114, pp. 813–18.
21. T.H. Okabe, K. Hirota, E. Kasai, F. Saito, Y. Waseda, and K.T. Jacob: *J. Alloys Compd.*, 1998, vol. 279, pp. 184–91.
22. K. Hirota, T.H. Okabe, F. Saito, Y. Waseda, and K.T. Jacob: *J. Alloys Compd.*, 1999, vol. 282, pp. 101–08.
23. G.Z. Chen, D.J. Fray, and T.W. Farthing: *Metall. Mater. Trans. B*, 2001, vol. 32B, pp. 1041–52.
24. J.-M. Oh, B.-K. Lee, C.-Y. Suh, S.-W. Cho, and J.-W. Lim: *Powder Metall.*, 2012, vol. 55, pp. 402–04.
25. J.-M. Oh, K.-M. Roh, B.-K. Lee, C.-Y. Suh, W. Kim, H. Kwon, and J.-W. Lim: *J. Alloys Compd.*, 2014, vol. 593, pp. 61–66.
26. K.-M. Roh, C.-Y. Suh, J.-M. Oh, W. Kim, H. Kwon, and J.-W. Lim: *Powder Technol.*, 2014, vol. 253, pp. 266–69.
27. O. Kubaschewski and W.A. Dench: *J. Inst. Met.*, 1953, vol. 82, pp. 87–91.
28. T. Yahata, T. Ikeda, and M. Maeda: *Met. Trans. B*, 1993, vol. 24, pp. 599–604.
29. S.-M. Han, Y.-S. Lee, J.-H. Park, G.-S. Choi, and D.-J. Min: *Mater. Trans.*, 2009, vol. 50, pp. 215–18.
30. Y. Su, L. Wang, L. Luo, X. Jiang, J. Guo, and H. Fu: *Int. J. Hydrog. Energy*, 2009, vol. 34, pp. 8958–63.
31. J. Reitz, C. Lochbichler, and B. Friedrich: *Intermetallics*, 2011, vol. 19, pp. 762–68.
32. M. Bartosinski, S. Hassan-Pour, B. Friedrich, S. Ratiev, and A. Ryabtsev: *Mater. Sci. Eng.*, 2016, vol. 143, p. 012009.
33. J.-M. Oh, H. Kwon, W. Kim, and J.-W. Lim: *Thin Solid Films*, 2014, vol. 551, pp. 98–101.
34. J.-M. Oh, I.-H. Choi, C.-Y. Suh, H. Kwon, J.-W. Lim, and K.-M. Roh: *Met. Mater. Int.*, 2016, vol. 22, pp. 488–92.
35. S.-J. Kim, J.-M. Oh, and J.-W. Lim: *Met. Mater. Int.*, 2016, vol. 22, pp. 658–62.
36. J.-M. Oh, K.-M. Roh, and J.-W. Lim: *Int. J. Hydrog. Energy*, 2016, vol. 41, pp. 23033–41.
37. Y. Zhang, Z.Z. Fang, Y. Xia, Z. Huang, H. Lefler, T. Zhang, P. Sun, M.L. Free, and J. Guo: *Chem. Eng. J.*, 2016, vol. 286, pp. 517–27.
38. Y. Zhang, Z.Z. Fang, P. Sun, T. Zhang, Y. Xia, C. Zhou, and Z. Huang: *J. Am. Ceram. Soc.*, 2016, vol. 138, pp. 6916–19.
39. Y. Xia, Z.Z. Fang, P. Sun, Y. Zhang, T. Zhang, and M. Free: *J. Mater. Sci.*, 2017, vol. 52, pp. 4120–28.
40. Y. Zhang, Z.Z. Fang, Y. Xia, P. Sun, B.V. Devener, M. Free, H. Lefler, and S. Zheng: *Chem. Eng. J.*, 2017, vol. 52, pp. 299–310.
41. Y. Xia, Z.Z. Fang, Y. Zhang, H. Lefler, T. Zhang, P. Sun, and M. Free: *Mater. Trans.*, 2017, vol. 58, pp. 355–60.
42. G.Z. Chen, D.J. Fray, and T.W. Farthing: *Nature*, 2000, vol. 407, pp. 361–64.
43. K. Ono and R.O. Suzuki: *JOM*, 2002, vol. 54, pp. 59–61.
44. H. Tamamura: *J. Surf. Finish. Soc. Jpn*, 2009, vol. 60, pp. 474–79 (in Japanese).
45. E. Nakamura: *Molten Salts*, 2015, vol. 58, pp. 119–26 (in Japanese).
46. L.Z. Zhao, Z.H. Zhang, S.Z. Jiao, and W.H. Liu: *Chin. Rare Earths*, 1986, vol. 6, pp. 44–49 (in Chinese).
47. W.P. Deng, X.D. Zheng, and X.D. Chi: *Chin. Rare Earths*, 1997, vol. 18, pp. 57–60 (in Chinese).
48. S.M. Pang, S.H. Yan, Z.A. Li, D.H. Cheng, H.L. Xu, and B. Zhao: *Chin. J. Rare Met.*, 2011, vol. 35, pp. 440–50 (in Chinese).
49. Y.B. Patrikeev, G.I. Novikov, and V.V. Badovskii: *Russ. J. Phys. Chem.*, 1973, vol. 47, p. 284.
50. D.D. Wagman, W.H. Evans, V.B. Parker, R.H. Schumm, I. Halow, S.M. Bailey, K.L. Churney, and R.L. Nuttall: *J. Phys. Chem. Ref. Data*, 1982, vol. 11.
51. O. Knacke, O. Kubaschewski, and K. Hesselman: *Thermochemical Properties of Inorganic Substances*, Springer-Verlag, Berlin, 1991.
52. F. Habashi ed.: *Handbook of Extractive Metallurgy*, VCH Verlagsgesellschaft mbH, Weinheim, Germany, 1997, pp. 1129–80.
53. C.J. Rosa: *Metall. Trans.*, 1970, vol. 1, pp. 2517–22.